

Immobilization of cobalt doped rutile TiO₂ on carbon nanotubes walls for efficient photodegradation of 2,4-dichlorophenol under visible light

Pejman Monazzam¹, Azadeh Ebrahimian Pirbazari^{2,*}, Behnam Fakhari Kisomi³, Ziba Khodaei⁴

¹ Faculty of Caspian, College of Engineering, University of Tehran, P.O. Box 43841-119, Rezvanshahr 43861-56387, Iran

²Hybridnanomaterials and Environment Laboratory, Faculty of Fouman, College of Engineering, University of Tehran, P.O. Box 43515-1155, Fouman 43516-66456, Iran

³ Faculty of Chemical Engineering, College of Engineering, University of Tehran, P.O. Box: 14155-6619, Tehran 4563-11155, Iran

⁴University of Applied Science and Technology, P.O. Box 41635-3697, Guilan, Iran

*Corresponding author at: Faculty of Fouman, College of Engineering, University of Tehran, P.O.Box 43515-1155, Fouman 43516-66456, Iran. Tel.: +981334734927; Fax: +981334737228. E-mail address: aebrahimian@ut.ac.ir (Azadeh Ebrahimian Pirbazari)

Abstract

In this work, we focused on improvement of rutile-type TiO₂ degradation efficiency by cobalt doping and decorating on carbon nanotubes walls (CNTs) (Co-TiO₂/CNTs). X-ray diffraction (XRD), energy dispersive X-ray spectroscopy (EDX), field emission scanning electron microscopy (FESEM), diffuse reflectance spectroscopy (DRS), and nitrogen physisorption were used to characterize the prepared samples. The XRD results indicated after cobalt doping, we obtained rutile phase as the major phase for cobalt containing samples. The band gap energy of the synthesized samples were calculated by Kubelka-Munk equation using diffuse reflectance spectra. The surface area of the samples was obtained by BET model and average pore diameter and pore volume of the samples were extracted from desorption branch of BJH model. The effectiveness of the samples was examined through degradation of 2,4-dichlorophenol (2,4-DCP) as a model of organic pollutants under visible light. We achieved 27% and 50% visible light degradation of 2,4-DCP in the presence of pure TiO₂ and Co-TiO₂/CNTs after 180 min irradiation, respectively. The high visible light activity of Co-TiO₂/CNTs sample can be approved that the presence of cobalt and CNTs reduce the band gap energy and sensitize TiO₂ surface to visible light respectively. The mechanism for degradation of 2,4-DCP by Co-TiO₂/CNTs photocatalyst under visible light is proposed.

Keywords: Cobalt; CNTs; Rutile; TiO₂; visible light degradation; 2,4-dichlorophenol

1. Introduction:

The expansion of degradation efficiency of TiO₂ in the visible light region is essential for decontamination of water pollutants. Many researchers made the efforts on the alteration of TiO₂ for improving of its efficiency under visible light by doping of noble, transition and rare earth metals [1, 2] and immobilization on different supports including zeolite, alumina, activated carbon and carbon nanotubes (CNTs)[3-5]. Another objective of surface modification of TiO₂ is to restrain the electrons and holes recombination by encouraging the charge isolation to improve the degradation performance [6, 7]. Cobalt as one of the most valuable dopants among the transition metals can develop the light response and degradation activity of TiO₂. Recently,

Ebrahimian et al. [8] prepared cobalt doped TiO₂ nanoparticles by hydrothermal method and the synthesized samples showed a great absorption range in the visible region. Iwasaki et al. [9] reported that doping of Co²⁺ into TiO₂ lattice could extend the absorption edge of TiO₂ and improve degradation performance of it under UV irradiation and visible light. The degradation performance of TiO₂ can be improved under UV by using CNTs in TiO₂ composite and surface features are changed to attain sensitivity to visible light [10]. Moreover, using CNTs in the structure of TiO₂ composite changes morphology and the particle dimension of TiO₂ [11]. Furthermore, the photocatalytic activity is greatly affected by CNTs as dispersing agent, adsorbent and photosensitizer [12].

The one dimensional nature of CNTs provides easy movement of charge carriers through nanotubes with no scattering causing ballistic transport that minimizes Joule heating and consequently, currents with very large densities transfer easily [13]. These transporting features of CNTs causes a suitable means of directing the flow of photoinduced electrons and holes and increase the life of them [14].

In our previous study [15], we investigated the effect of cobalt doping on the phase formation of TiO₂ and achieved anatase as the major phase for the prepared nanocomposites. In the current study, we focused on the synthesis of cobalt doped TiO₂ with rutile major phase and decorated on the walls of CNTs. The textural and morphology features of the obtained photocatalysts were characterized by XRD, FTIR, DRS, FESEM/EDX and N₂ physisorption analyses. The effectiveness of the obtained samples was assessed through degradation of synthetic wastewater containing 2,4-dichlorophenol (2,4-DCP) under visible light.

2. Materials and Methods

2.1. Materials and reagents

Cobalt (II) chloride hexahydrate (CoCl₂.6H₂O) (Merck, No.102539), Titanium isopropoxide (TIP) (Merck No. 8.21895), ethanol (Merck No. 818760), high-purity 2,4-DCP, 98%, (Merck No. 803774), and carboxylic groups-functionalized CNTs with diameter of the 10-20 nm and the

length of 0.5-2.0 μm provided by Neutrino Corporation (Iran) were used in this study. Deionized water was used in all experiments.

2.2. Preparation of Co-TiO₂/CNTs nanocomposite

Co-TiO₂/CNTs photocatalyst was synthesized through a modified sol-gel technique. 0.96 g of CoCl₂.6H₂O, 20 mL TIP and 60 mL ethanol were agitated for 2h (Solution A). Next, solution B, 40 mL ethanol, 10 mL deionized water, 4 mL hydrochloric acid and 0.08 g CNTs were poured into the solution A and agitated for 12h at ambient temperature. The sol was generated after stirring for 12h and aging at ambient temperature for 24h. Then it was evaporated at 80 °C for 8h to obtain the dried powder. Lastly, the Co-TiO₂/CNTs sample was obtained by calcinating the resulted powder at 450 °C under air for 2h. Pure TiO₂, Co-TiO₂ and TiO₂/CNTs samples were prepared through the similar method (Table 1).

2.3. Characterization

The XRD analysis was performed using a Siemens D5000 instrument (Germany) while Cu K α radiation was employed as the X-ray source. The diffractograms were recorded in the $2\theta = 20 - 80^\circ$. Morphology of the samples was identified by scanning electron microscopy (SEM) (Vegall-Tescan Company), which was coupled with an energy dispersive X-ray (EDX) detector. The diffuse reflectance UV-Vis spectra (DRS) of the samples were recorded by an Ava Spec-2048TEC spectrometer. Physisorption of nitrogen was studied by a Quantachrome Autosorb-1-MP (Micromeritics) in order to measure BET areas through static nitrogen physisorption. The samples were degassed at 200 °C for 2 h prior to the sorption measurement.

2.4. Photodegradation of 2,4-DCP

We selected 2,4-DCP as a model of organic pollutants to examine degradation performance of the obtained samples. We used Halogen, ECO OSRAM 500W lamp (350 to 800 nm, with the most intense peak at 575 nm) as visible light source. In each degradation experiment, the beaker containing optimum amount of photocatalyst and 100 mL 2,4-DCP aqueous solution (40 mg/L) was agitated first for 10 min, in the dark, for adsorption/ desorption equilibrium and after this

time, the lamp turned on for 180 min. At certain times, 2 mL of the solution was taken and filtered to eliminate the photocatalyst and analyzed using Rayleigh UV-2601 UV/VIS spectrophotometer ($\lambda_{\max}= 227\text{nm}$).

3. Results&Discussion

3.1. X-ray diffraction analysis

The XRD patterns of the synthesized samples have been presented in Fig. 1. In XRD pattern of pure TiO_2 (Fig. 1a), the diffractions at $2\theta= 27.48^\circ, 36.14^\circ, 41.24^\circ$ and 54.34° with Miller indexes (110), (101), (111) and (211), respectively are the main diffractions of polycrystalline with a rutile structure[16]. The diffractions at $2\theta= 37.80^\circ, 48.18^\circ,$ and 54.09° are the key peaks for the anatase crystalline phase of TiO_2 (JCPDS 21-1272). The XRD pattern showed the synthesized TiO_2 comprising predominant rutile crystalline phase and a small amount of anatase crystalline phase. Moreover, the XRD pattern of Co- TiO_2 sample (Fig. 1b) did not indicate any cobalt phase, so it can be concluded that cobalt ions homogenously dispersed into the TiO_2 crystallites and represented rutile phase as major phase for TiO_2 [17, 18].

In XRD pattern of TiO_2/CNTs (Fig. 1c), the main diffraction of CNTs at $2\theta=25.5^\circ$ [19] has not been detected and it may be overlapped with the main diffraction of anatase TiO_2 at $2\theta=25.3^\circ$. Furthermore, it may be attributed to the significant difference between the mass percent of CNTs and TiO_2 and the low crystallinity of CNTs [13]. In the XRD pattern of Co- TiO_2/CNTs (Fig. 1d), the main diffractions of rutile crystalline phase were detected for TiO_2 .

The mean TiO_2 crystal size for each samples was calculated at $2\theta= 27.48^\circ$ by using Scherrer's equation (Eq. (1))[20]:

$$D= K\lambda/\beta \cos\theta \quad (\text{eq. 1})$$

Where D represents the mean crystallite size of TiO_2 in nm, λ is the wavelength of X-ray (1.54056 \AA), β refers to the diffraction full width at half maximum (FWHM) in radian, K represents a coefficient (0.89) and θ is the diffraction angle at $2\theta= 27.48^\circ$. The TiO_2 crystal size for all the obtained samples is in the nanosized range (Table 2).The mean crystallite size of TiO_2 in Co- TiO_2 and Co- TiO_2/CNTs samples is smaller compared with pure TiO_2 , it can be stated that adding cobalt

to titania delays the growth of TiO₂ nanoparticles. It seems that cobalt ions form complex with the TiO₂ surface oxygen, hence, suppress the growth of TiO₂ crystallite[21].

The lattice parameters ($a=b\neq c$) of tetragonal crystalline structure were obtained for (110) crystal plane of rutile phase using Eq. (2):

$$1/d^2 = (h^2 + k^2)/a^2 + l^2/c^2 \quad (\text{eq. 2})$$

Considering the interplanar spacing (d_{hkl}), the distance between adjacent planes in the set (hkl) can be determined using the Bragg law (Eq. (3)):

$$d_{hkl} = \lambda/2 \sin\theta \quad (\text{eq. 3})$$

The volume of cell (tetragonal one) was computed by Eq. (4):

$$V = a^2c \quad (\text{eq. 4})$$

Where a and c are considered lattice factors. Table 2 displays the lattice factors of the synthesized samples. The achieved values for the lattice factors of TiO₂ in the synthesized samples matched well with the TiO₂ rutile structure [16]. The calculated values for the lattice factors of pure TiO₂ are in well matched with the rutile phase of TiO₂ [16]. No other impurity peaks are detected, which ensure high purity of TiO₂ powder used for Co doping. The diffraction patterns of the synthesized samples do not show any extra peaks confirming that the rutile phase is not troubled upon Co doping in TiO₂. A significant difference between ionic radii of the dopant and the host ions (i.e., Co²⁺: 0.745 Å and Ti⁴⁺: 0.605 Å, with a coordination number of 6) is predictable to cause a small enhancement of the TiO₂ unit cell size.

3.2. Diffuse reflectance analysis

The solid-state UV-Visible spectra (Fig. 2A) were recorded for all the samples.

In the DR spectrum of pure TiO₂, absorption peak around 400 nm can be attributed to the charge-transfer from the valence band of the oxide anions to the conduction band of the Ti⁴⁺cations [21].

The diffuse reflectance spectra of the Co-TiO₂ and Co-TiO₂/CNTs samples (Figs. 2b, d), consist of additional broad absorption peak between 500 to 750 nm. The genesis of absorption peak is attributed to Co²⁺/Ti⁴⁺ charge-transfer interaction [22]. This may also be a reason for high degradation efficiency of these samples in the visible region compared with pure TiO₂.

We also measured the energy of band gap of the synthesized samples using the diffuse reflectance spectra according to Eq. (5)[23].

$$[F(R) \text{ } h\nu]^{0.5} = A (h\nu - E_{bg}) \quad (\text{eq. 5})$$

Where A is constant, F(R) is the function of Kubelka-Munk (Fig. 2B), and E_{bg} is the band gap. The E_{bg} data of samples have been presented in Table 3. The pure TiO₂ showed high reflection within the visible light region (>400 nm), while the samples comprising cobalt showed lower reflection in the visible region, meaning that visible light photoresponse of the cobalt doped samples was increased. Red shifts found for the cobalt doped TiO₂ samples showed that the band gap energy of the samples was decreased gradually (Table 3). The band gap of samples containing cobalt decreased compared with TiO₂. It can be clearly seen that doping cobalt in the TiO₂ structure affects the optical features of TiO₂ significantly. It is evident that, the degradation activity of the Co-TiO₂ and Co-TiO₂/CNTs is greatly shifted into the visible light region, and exhibits a band gap narrowing 2.375 and 2.200 eV compared with that of pure TiO₂ (2.880 eV). It is explained in literature that the presence of transition metals might introduce new intra band gap states, giving the TiO₂ the capacity to absorb light at lower energy levels, thus, promoting the absorption on the visible part of the spectrum. The incorporation of the transition metal provides d orbitals just below the conduction band. These d orbitals are then able to receive electrons from the valence band, thus lowering the band gap energy[24].

3.3. FESEM/EDX and TEM analyses

Fig. 3 displays the FESEM images of the synthesized samples. FESEM images show that all the samples are slightly agglomerated and in the case of TiO₂/CNTs and Co-TiO₂/CNTs samples (Figs. 3c, d), TiO₂ and Co-TiO₂ nanoparticles are decorated on the CNTs walls. The FESEM analysis and

XRD calculations (Table 2) display that the existence of cobalt and CNTs has prevented increasing the dimension of TiO_2 particles (Table 2).

The EDX results were utilized to study the elemental composition of the samples (Fig. 4 and Table 4). The elemental analysis confirms the existence of C, Ti, O and Co elements in these samples. The EDX patterns of the samples (Fig. 4) display two peaks about 0.2 and 4.5 keV. The strong peak is related to the bulk TiO_2 and the less strong one is related to the surface TiO_2 . Fig. 4 shows the peaks of cobalt at 0.6, 6.9 and 7.5 keV. The less strong peak is allocated to cobalt in the TiO_2 lattices[21, 25]. Fig. 5 demonstrates elemental mapping images of the synthesized samples. According to the elemental mapping mode, cobalt was greatly and homogeneously dispersed in the TiO_2 lattice. This implies good interaction of cobalt and TiO_2 over the sol-gel synthesis procedure. The elemental analysis of the samples showed the existence of cobalt atoms and CNTs in the powder structure, as the opposite of XRD patterns.

Fig. 6 shows the TEM image of Co- TiO_2 /CNTs nanocomposite. According to these images, Co- TiO_2 NPs are dispersed on the wall of CNTs.

3.4. N_2 physisorption analysis

The results of N_2 adsorption/desorption isotherms are shown in Fig.7. The sorption isotherms for the prepared samples correspond to the type IV isotherm based on the classification of IUPAC[26]. Textural and structural parameters of the obtained samples have been presented in Table 5. The specific surface areas calculated according to BET and the average pore diameter and pore volumes were extracted from the desorption branch based on the BJH model. Cobalt addition resulted in a reduction in both surface area and pore volume for the Co- TiO_2 and Co- TiO_2 /CNTs samples. These variations could be attributed to the developed sintering and/or agglomeration of TiO_2 or to the formation of CoTiO_3 compound[22].

3.5. Degradation of 2,4-DCP

The degradation activity of 2,4-DCP with the synthesized samples under visible light presented in Fig. 8. Amongst the prepared samples, the photocatalytic activity of the Co- TiO_2 /CNTs was the

maximum and 50% degradation of 2,4-DCP achieved following 180 min irradiation under visible light. In the same conditions, we obtained 27%, 32% and 35% degradation of 2,4-DCP in the presence of pure TiO₂, Co-TiO₂ and TiO₂/CNTs samples respectively.

The two basic factors that are responsible for the activity of photocatalysts include surface area and light absorption capacity[21]. The DRS analysis results (Fig. 2) show that light absorption capacities of the prepared samples are different and increase with addition of cobalt in visible region. Therefore, addition of cobalt has two opposite effects on the degradation activity of the samples; increasing light absorption capacity and decreasing surface area. The degradation activity depends on which one of these is the dominant factor[8].

The higher degradation activity of Co-TiO₂/CNTs can be noticed that the presence of CNTs and cobalt clearly led to a synergetic impact on 2,4-DCP degradation and caused a larger photocatalytic performance. The more degradation activity of Co-TiO₂/CNTs nanocomposite may be described as firstly, the Co doped into TiO₂ could efficiently capture the photo-induced electrons and holes, which controlled combining photoinduced charge carriers and increased the degradation performance. Secondly, there are more surface hydroxyl groups in Co-TiO₂/CNTs samples compared with the pure TiO₂ which would be helpful for 2,4-DCP adsorption. The creation of hydroxyl radicals could be facilitated by the abundant hydroxyl groups adsorbed on the catalyst surface that could optimize the degradation procedure of the 2,4-DCP adsorbed on the surface[5]. Moreover, there is a synergetic impact among CNTs and TiO₂, and CNTs playing role as a photosensitizer. The photo-induced electrons can be trapped by CNTs and so, superoxide radical ion and/or hydroxyl radical is formed on the TiO₂ surface that they play role in degrading the organic compound. It can be suggested that charge on the surface of TiO₂ in the combined catalysts is increased due to the presence of CNTs. The surface charge may cause alterations of the fundamental procedure of electron/hole pair creation while using visible light [13]. Therefore, it may be the single interaction between TiO₂ and CNTs that endows the ternary nanocomposite with a higher catalytic activity in the degradation of 2,4-DCP than pure TiO₂. In the case of samples comprising cobalt, the Co²⁺ trapped electrons which then moved to be absorbed O₂ for reaching a greater photocatalytic activity. According to the literature [27], with the replacement for Ti⁴⁺ by Co²⁺ in TiO₂ crystal structure, the catalyst can introduce a new levels

of impurity to the conduction band of TiO_2 and the electrons can be moved from the valence band to these impurity levels, causing a narrowing of the band gap. This fact shows the presence of higher number of photogenerated electrons and holes which can be introduced for participating in the photocatalytic reactions [28]. Though, recombining photogenerated electrons and holes is one of the most important parameters that decline the photoactivity of the TiO_2 catalyst. Any parameter, which suppresses the recombination of electron-hole, will increase the photocatalytic performance [29]. Generally, if the dimension of doping metal ion is very similar to Ti^{4+} , entering metal ion into the TiO_2 crystal interstitial site is very probable. The doping metal ion placed mostly on the shallow surface of TiO_2 can induce defects. These defects can become the centers of shallow electrons or holes traps, which would powerfully progress separation process of an electron-hole pair. Therefore, the photocatalyst will have a great photocatalytic performance[30]. Our suggested mechanism for photodegradation of 2,4-DCP by Co- TiO_2 /CNTs photocatalyst is shown in Fig.9.

4. Conclusions

In summary, the photocatalytic efficiency of rutile-type TiO_2 was successfully improved by cobalt doping and decorating on CNTs walls. It was found that the Co- TiO_2 /CNTs sample presented enhanced degradation of 2,4-dichlorophenol (2,4-DCP) and exhibited expansion in spectral response range shifted to the visible region. We obtained 27% and 50% visible light degradation of 2,4-DCP in the presence of TiO_2 and Co- TiO_2 /CNTs respectively after 180min irradiation. The presence of CNTs and cobalt dopant in Co- TiO_2 /CNTs nanocomposite promoted the separation of photoinduced charge carriers and extended the absorption spectrum of TiO_2 into visible region.

Acknowledgements

The authors wish to acknowledge the financial support of University of Tehran for supporting of this research. Also, the author wish to acknowledge the financial support of Iran Nanotechnology Initiative Council (INIC) Foundation (Grant No: 122611).

References:

1. Sarteep Z, Pirbazari AE, Aroon MA, Silver Doped TiO₂ Nanoparticles: Preparation, Characterization and Efficient Degradation of 2,4-dichlorophenol Under Visible Light. *Journal of Water and Environmental Nanotechnology*. 2016;1;135-144.
2. Wang S, Zhou S, Photodegradation of methyl orange by photocatalyst of CNTs/P-TiO₂ under UV and visible-light irradiation. *Journal of hazardous materials*. 2011;185;77-85.
3. Saleh TA, Gondal M, Drmosh Q, Yamani Z, Al-Yamani A, Enhancement in photocatalytic activity for acetaldehyde removal by embedding ZnO nano particles on multiwall carbon nanotubes. *Chemical Engineering Journal*. 2011;166;407-412.
4. Zhang J, Huang Zh, Yong X, Kang Fy, Carbon-coated TiO₂ composites for the photocatalytic degradation of low concentration benzene. *New Carbon Materials*. 2011;26;63-70. 26 (2011).
5. Yang Q, Deng Y, Hu W, Preparation of alumina/carbon nanotubes composites by chemical precipitation. *Ceramics International*. 2009;35;1305-1310.
6. Feng H, Zhang MH, Liya EY, Hydrothermal synthesis and photocatalytic performance of metal-ions doped TiO₂. *Applied Catalysis A: General*. 2012;413;238-244.
7. Pasikhani JV, Gilani N, Pirbazari AE, Improvement the wastewater purification by TiO₂ nanotube arrays: The effect of etching-step on the photo-generated charge carriers and photocatalytic activity of anodic TiO₂ nanotubes. *Solid State Sciences*. 2018;84;57-74.
8. Pirbazari AE, Monazzam P, Kisomi BF, Co/TiO₂ nanoparticles: preparation, characterization and its application for photocatalytic degradation of methylene blue. *Desalination and Water Treatment*. 2017;63;283-292.
9. Iwasaki M, Hara M, Kawada H, Tada H, Ito S, Cobalt Ion-Doped TiO₂ Photocatalyst Response to Visible Light. *Journal of Colloid and Interface Science*. 2000;224;202-204.
10. Wang H, Wang HL, Jiang WF, Li ZQ, Photocatalytic degradation of 2, 4-dinitrophenol (DNP) by multi-walled carbon nanotubes (MWCNTs)/TiO₂ composite in aqueous solution under solar irradiation. *Water research*. 2009;43;204-210.
11. Huang B, Yang Y, Chen X, Ye D, Preparation and characterization of CdS–TiO₂ nanoparticles supported on multi-walled carbon nanotubes. *Catalysis Communications*. 2010;11;844-847.
12. Peining Z, Nair AS, Shengyuan Y, Ramakrishna S, TiO₂–MWCNT rice grain-shaped nanocomposites—Synthesis, characterization and photocatalysis. *Materials Research Bulletin*. 2011;46;588-595.
13. Wei B, Vajtai R, Ajayan P, Reliability and current carrying capacity of carbon nanotubes. *Applied Physics Letters*. 2001;79;1172-1174.
14. Xia XH, Jia ZJ, Yu Y, Liang Y, Wang Z, Ma LL, Preparation of multi-walled carbon nanotube supported TiO₂ and its photocatalytic activity in the reduction of CO₂ with H₂O. *carbon*. 2007;45;717-721.

15. Laghani SN, Pirbazari AE, Photocatalytic Treatment of Synthetic Wastewater Containing 2,4 dichlorophenol by Ternary MWCNTs /Co-TiO₂ Nanocomposite Under Visible Light. *Journal of Water and Environmental Nanotechnology*. 2017;2;290-301.
16. Ogata M, Kadowaki K, Ijiri M, Takemoto Y, Terashima K, Wakita T, Yokoya T, Muraoka Y, Effect of aliovalent dopants on the kinetics of spinodal decomposition in rutile-type TiO₂-VO₂. *Journal of the European Ceramic Society*. 2017;37;3177-3183.
17. Jiang P, Xiang W, Kuang J, Liu W, Cao W, Effect of cobalt doping on the electronic, optical and photocatalytic properties of TiO₂. *Solid State Sciences*. 2015;46;27-32.
18. Preethi T, Abarna B, Vidhya K, Rajarajeswari G, Sol-gel derived cobalt doped nano-titania photocatalytic system for solar light induced degradation of crystal violet. *Ceramics International*. 2014;40;13159-13167.
19. Ahmmad B, Kusumoto Y, Somekawa S, Ikeda M, Carbon nanotubes synergistically enhance photocatalytic activity of TiO₂. *Catalysis Communications*. 2008;9;1410-1413.
20. Khan M, Cao W, Cationic (V, Y)-codoped TiO₂ with enhanced visible light induced photocatalytic activity: A combined experimental and theoretical study. *Journal of Applied Physics*. 2013;114;183514.
21. Hamadani M, Reisi-Vanani A, Majedi A, Sol-gel preparation and characterization of Co/TiO₂ nanoparticles: application to the degradation of methyl orange. *Journal of the Iranian Chemical Society*. 2010;7;52-58.
22. Ganesh I, Gupta A, Kumar P, Sekhar PC, Radha K, Padmanabham G, Sundararajan G, Preparation and characterization of Co-doped TiO₂ materials for solar light induced current and photocatalytic applications. *Materials Chemistry and Physics*. 2012;135;220-234.
23. Kumar S, Khanchandani S, Thirumal M, A.K. Ganguli AK, Achieving enhanced visible-light-driven photocatalysis using type-II NaNbO₃/CdS core/shell heterostructures. *ACS applied materials & interfaces*. 2014;6;13221-13233.
24. Zhu J, Chen F, Zhang J, Chen H, Anpo M, Fe³⁺-TiO₂ photocatalysts prepared by combining sol-gel method with hydrothermal treatment and their characterization. *Journal of Photochemistry and Photobiology A: Chemistry*. 2006;180;196-204.
25. Venkatachalam N, Palanichamy M, Arabindoo B, Murugesan V, Enhanced photocatalytic degradation of 4-chlorophenol by Zr⁴⁺ doped nano TiO₂. *Journal of Molecular Catalysis A: Chemical*. 2007;266;158-165.
26. Sing KSW, Reporting physisorption data for gas/solid systems with special reference to the determination of surface area and porosity (Recommendations 1984). *Pure and applied chemistry*. 1985;57;603-619.
27. Yang J, Cui S, Qiao Jq, Lian Hz, The photocatalytic dehalogenation of chlorophenols and bromophenols by cobalt doped nano TiO₂. *Journal of Molecular Catalysis A: Chemical*. 2014;395;42-51.

28. Li CJ, Wang JN, Wang B, Gong JR, Lin Z, A novel magnetically separable TiO₂/CoFe₂O₄ nanofiber with high photocatalytic activity under UV–vis light. *Materials Research Bulletin*. 2012;47;333-337.
29. Sakthivel S, Shankar M, Palanichamy M, Arabindoo B, Bahnemann D, Murugesan V, Enhancement of photocatalytic activity by metal deposition: characterisation and photonic efficiency of Pt, Au and Pd deposited onTiO₂ catalyst. *Water research*. 2004;38;3001-3008.
30. Chand R, Obuchi E, Katoh K, Luitel HN, Nakano K, Effect of transition metal doping under reducing calcination atmosphere on photocatalytic property of TiO₂ immobilized on SiO₂ beads. *Journal of Environmental Sciences*. 2013;25;1419-1423.

Table 1. Nomenclature of the prepared samples

Samples	TIP (ml)	HCl (ml)	CoCl ₂ .6H ₂ O (g)	Ethanol (ml)	H ₂ O (ml)	CNTs (g)
TiO ₂	20	4	-	100	10	-
Co-TiO ₂	20	4	0.96	100	10	-
TiO ₂ /CNTs	20	4	-	100	10	0.08
Co-TiO ₂ /CNTs	20	4	0.96	100	10	0.08

Table 2. Phase, crystal size and lattice parameters of the prepared samples

Sample	Major Phase	Crystal size (nm)	a=b (Å)	c (Å)	Cell volume (Å ³)
TiO ₂	Rutile	21.540	4.598	2.957	62.505
Co-TiO ₂	Rutile	20.466	4.600	2.956	62.561
TiO ₂ /CNTs	Rutile	21.261	4.588	2.951	62.110
Co-TiO ₂ /CNTs	Rutile	18.190	4.593	2.951	62.266

Table 3. Color and band gap energy of the prepared samples

Samples	E_{bg} (eV)	Color
TiO ₂	2.880	White
Co-TiO ₂	2.375	Green
TiO ₂ /CNTs	2.970	Gray
Co-TiO ₂ /CNTs	2.200	Slime Green

Table 4. Elemental chemical analysis of the prepared samples.

Samples	Ti (wt%)	O (wt%)	Co (wt%)	C (wt%)	Cl (wt%)
TiO ₂	49.26	50.74	-	-	-
Co-TiO ₂	64.54	29.00	5.36	-	1.10
TiO ₂ /CNTs	44.88	47.66	-	7.46	-
Co-TiO ₂ /CNTs	37.16	53.03	3.15	4.50	2.15

Table 5. Textural and structural parameters of the prepared samples.

Sample	S_{BET} (m^2/g)	Average pore diameter (nm)	Pore volume (cm^3/g)
TiO ₂	41.21	19.02	0.20
Co-TiO ₂	34.28	25.75	0.13
TiO ₂ /CNTs	46.84	21.10	0.25
Co-TiO ₂ /CNTs	33.70	17.27	0.15

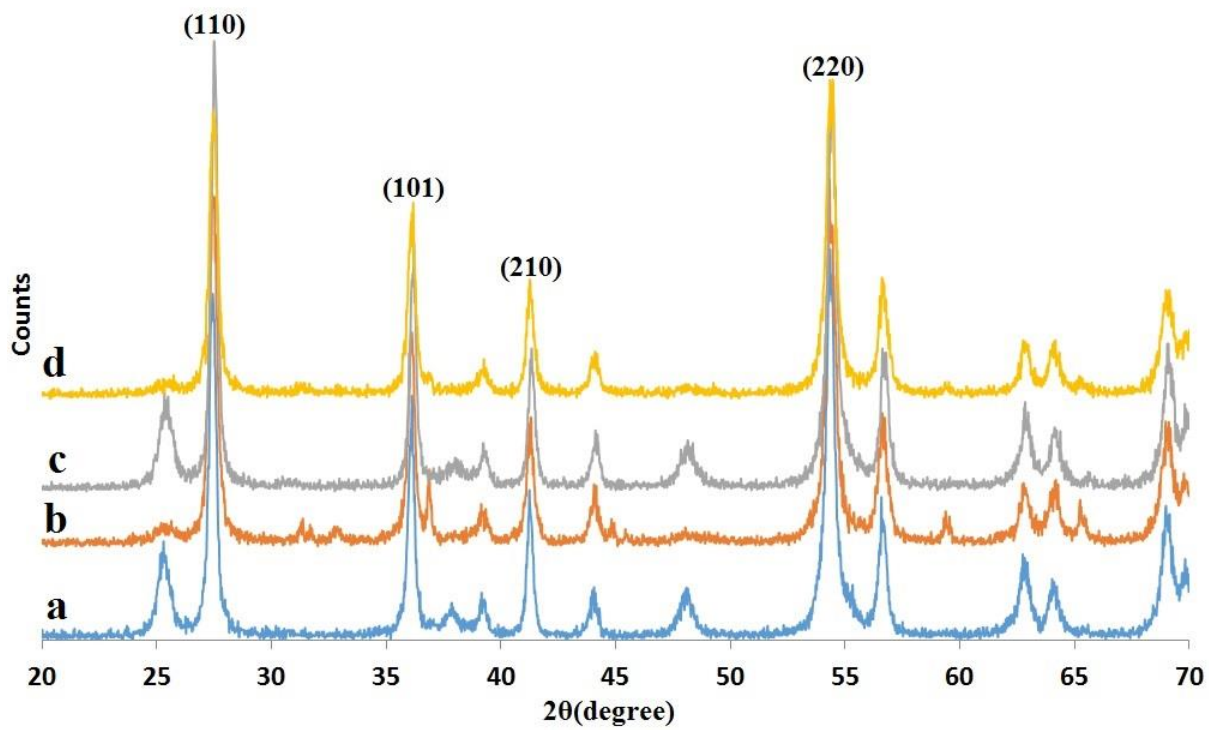


Fig. 1 The XRD patterns of a) TiO₂, b) Co-TiO₂, c) TiO₂/CNTs and d) Co-TiO₂/CNTs

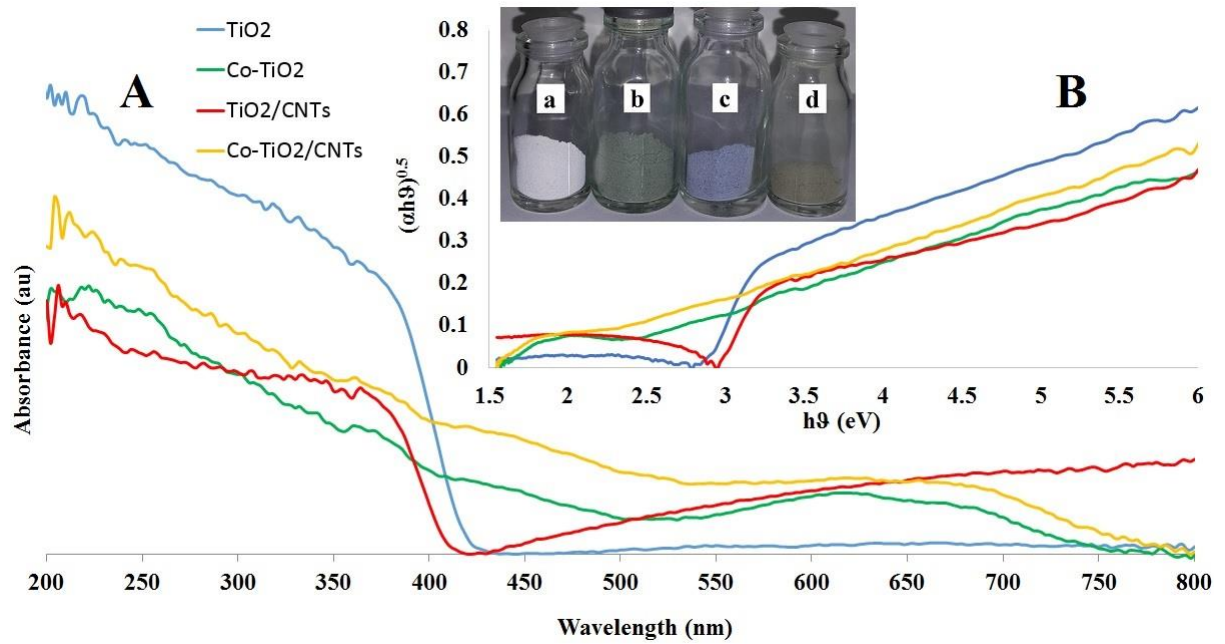


Fig. 2 A: Diffuse reflectance spectra and B: Kubelka-Munk plots for the band gap energy calculation of a)TiO₂ b)Co-TiO₂ c) TiO₂/CNTs and d) Co-TiO₂/CNTs.

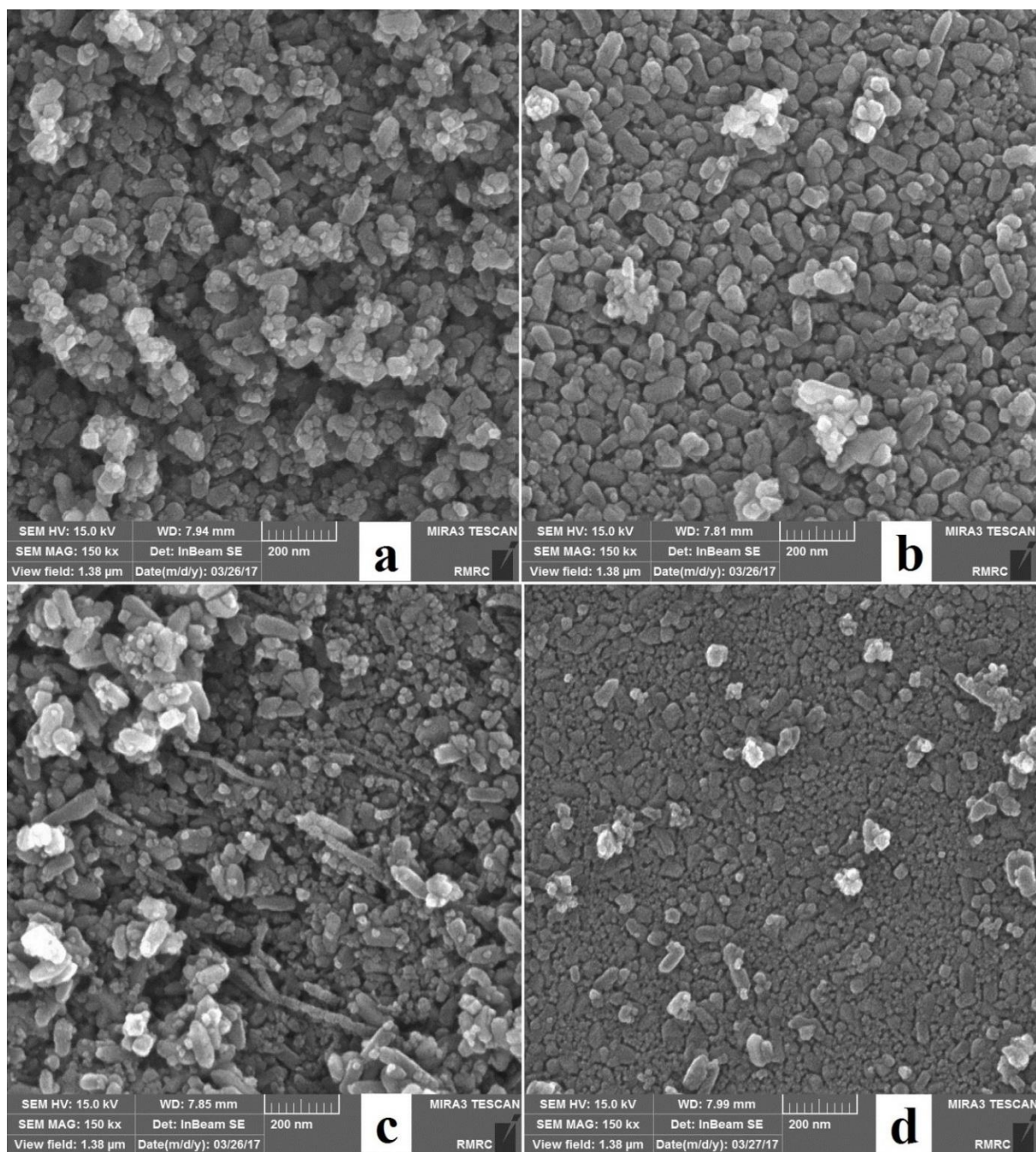


Fig. 3 FESEM images of a) TiO₂, b) Co-TiO₂, c) TiO₂/CNTs and d) Co-TiO₂/CNTs

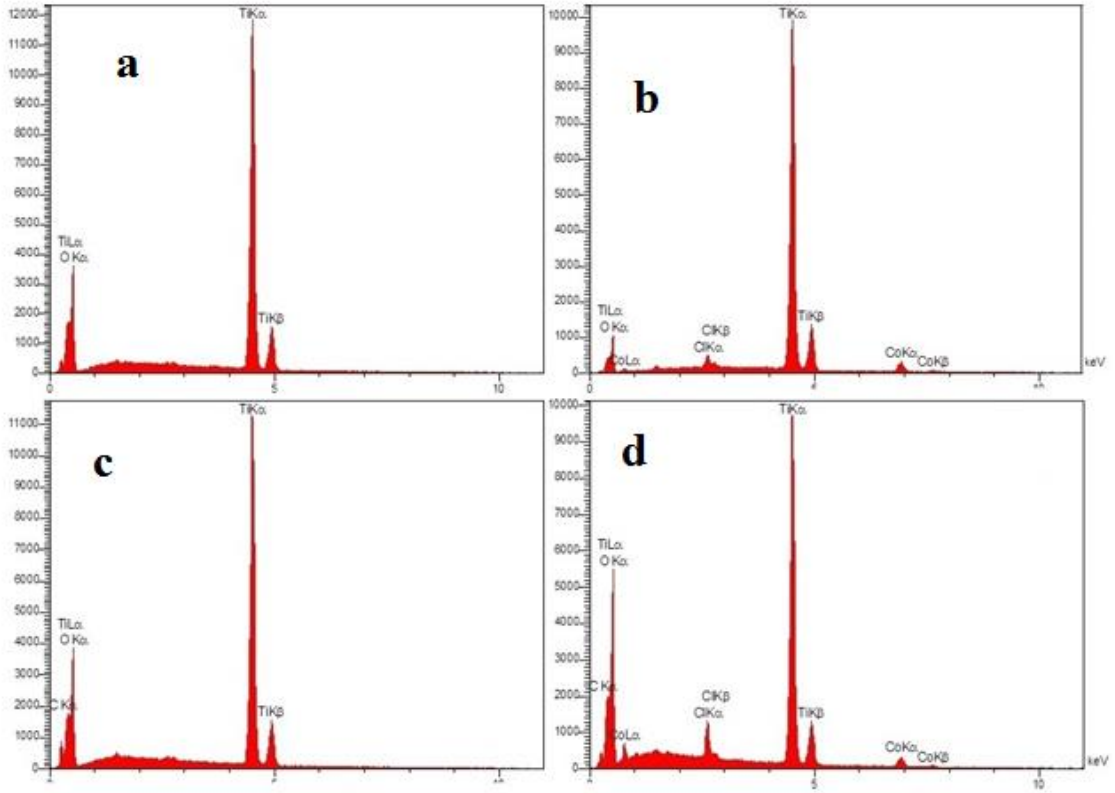


Fig. 4 EDX spectra of a) TiO₂, b) Co-TiO₂, c) TiO₂/CNTs and d) Co-TiO₂/CNTs

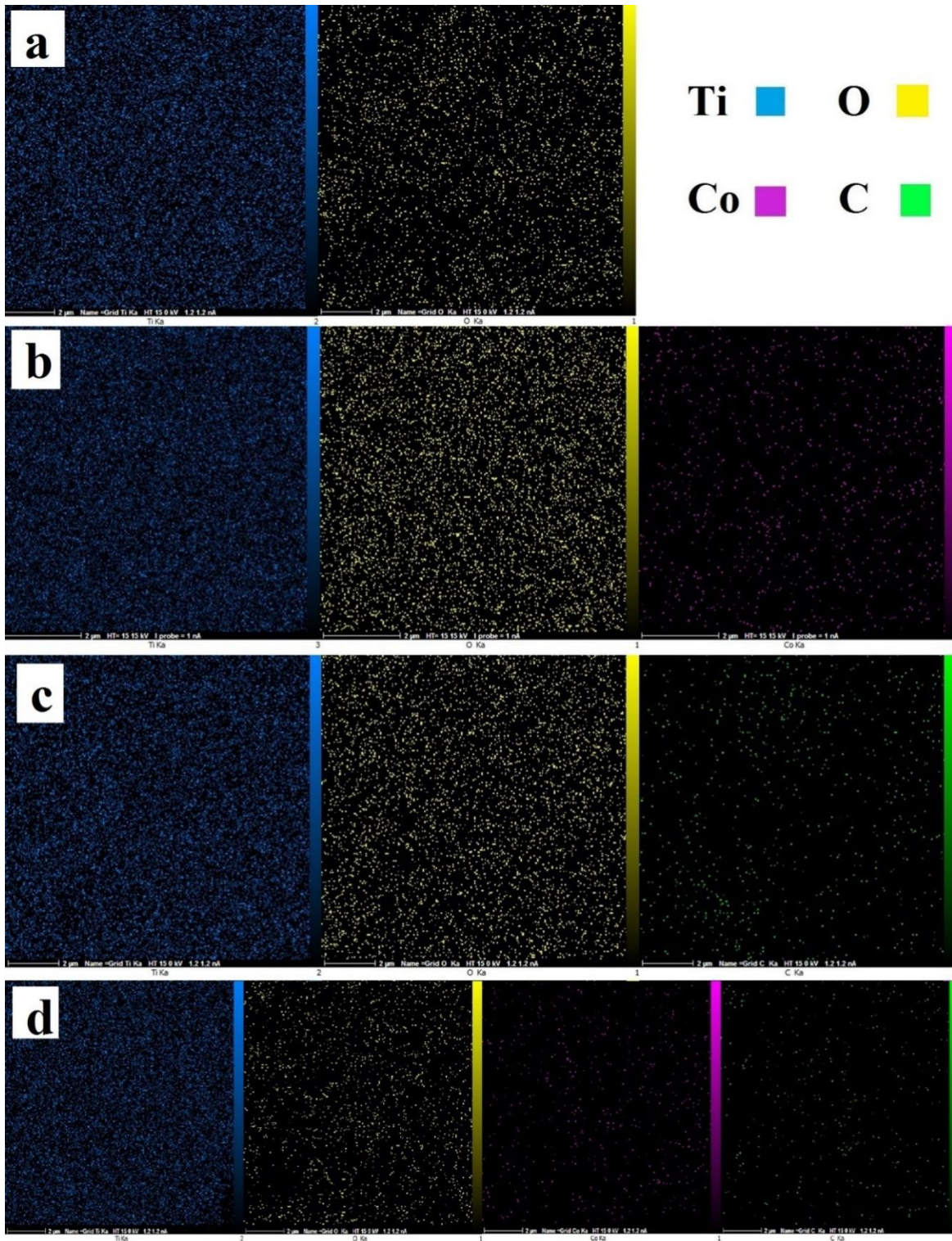


Fig. 5 Elemental mapping of a) TiO₂, b) Co-TiO₂, c) TiO₂/CNTs and d) Co-TiO₂/CNTs

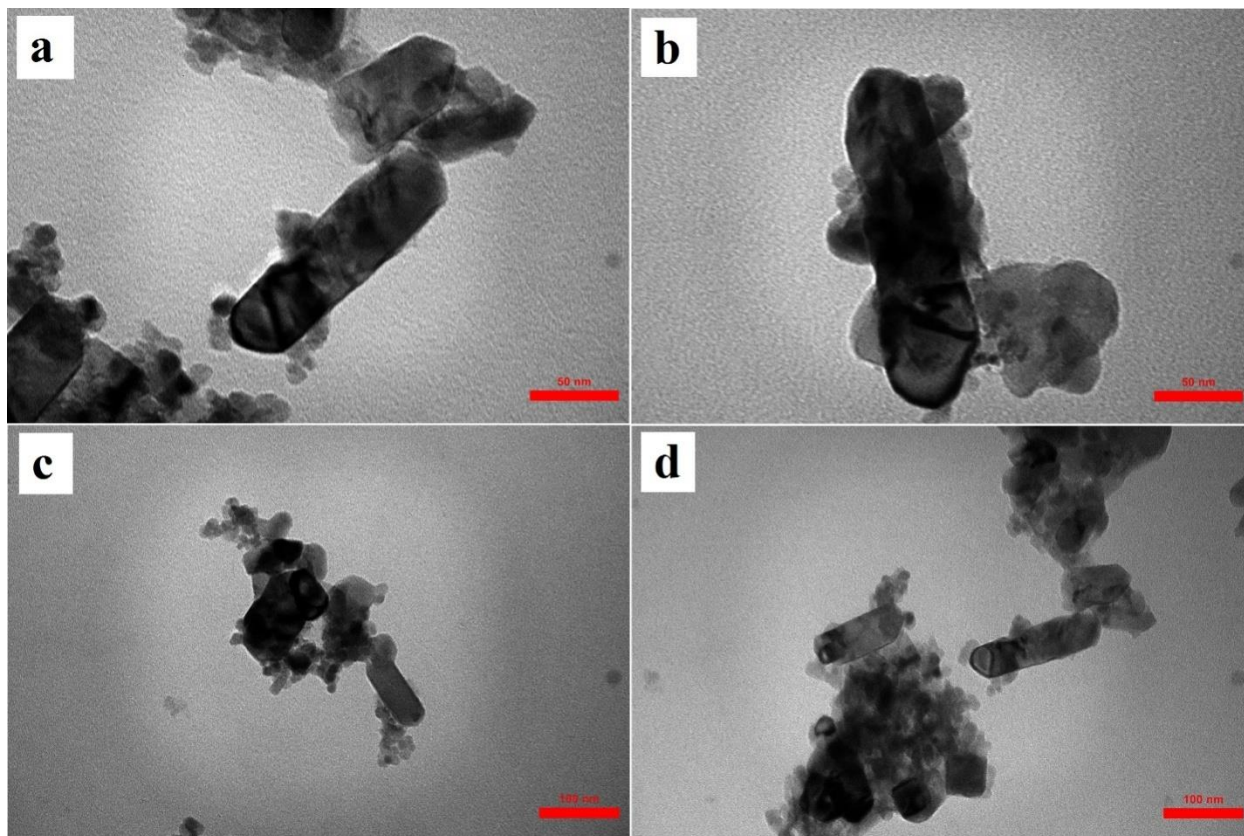


Fig. 6 TEM images of Co-TiO₂/CNTs nanocomposite at a, b) 50 nm and c, d) 100 nm

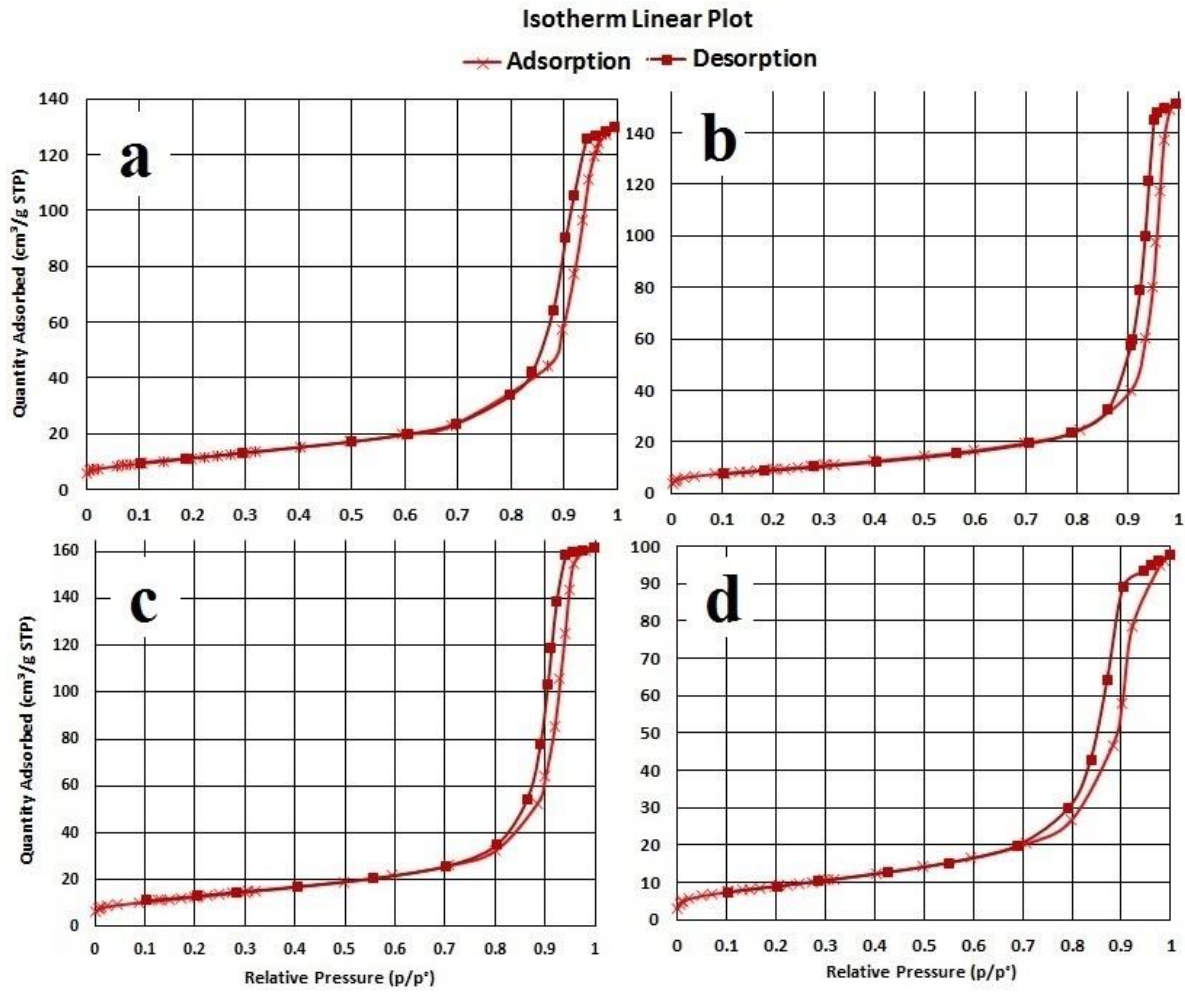


Fig. 7 N_2 adsorption–desorption isotherms for a) TiO_2 , b) Co-TiO_2 , c) TiO_2/CNTs and d) $\text{Co-TiO}_2/\text{CNTs}$

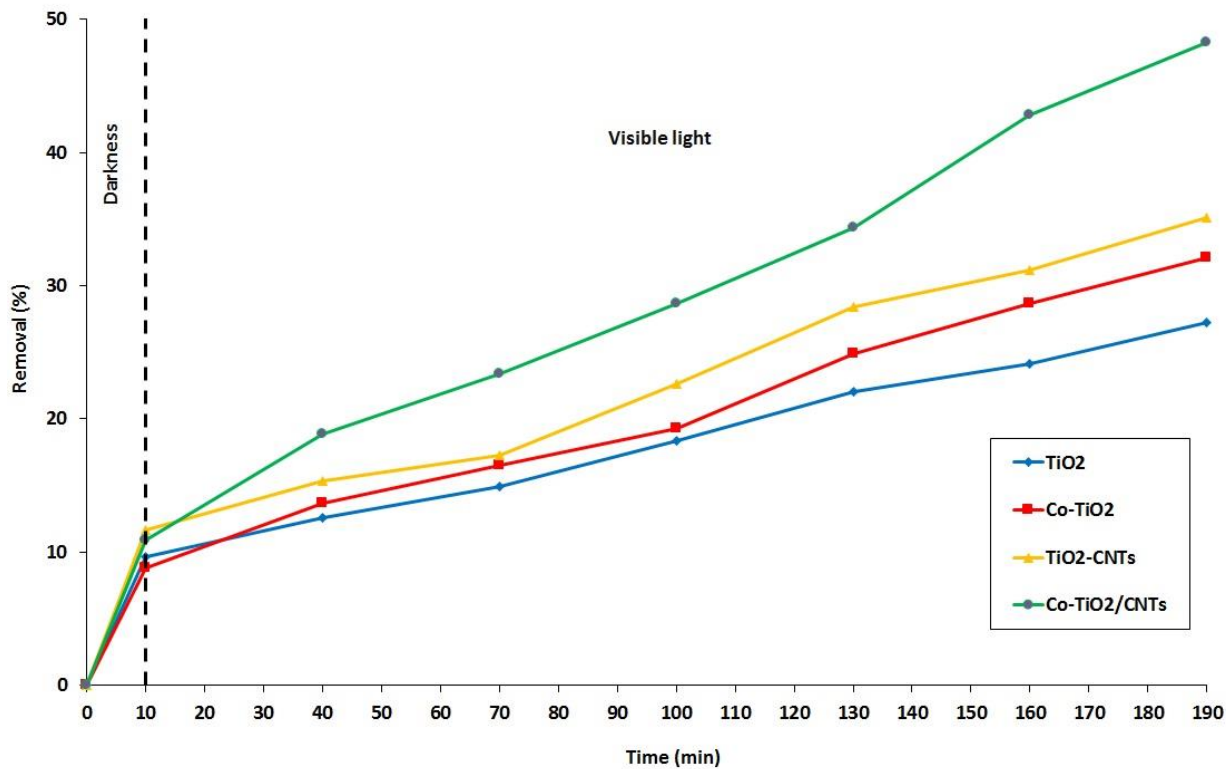


Fig. 8 Photodegradation of 2,4-DCP in the presence of the prepared samples under visible light. (Initial concentration of 2,4-DCP, 40 mg /L; volume, 100 mL; catalyst dosage, 10 mg and Irradiation time: 180 min).

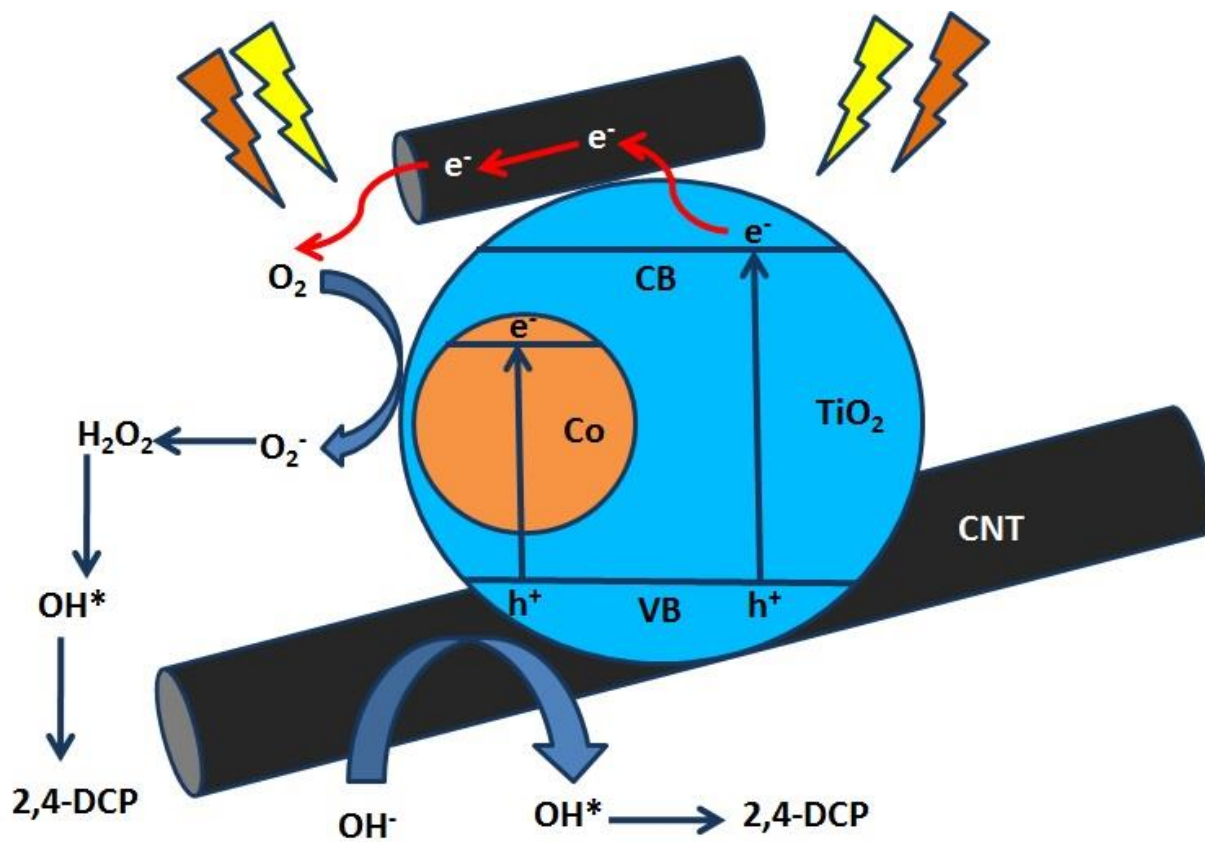


Fig .9 Suggested mechanism for 2,4-DCP degradation in the presence of Co-TiO₂/CNTs under visible light.